Transient optomechanically induced transparency in a silica microsphere

Chunhua Dong, Victor Fiore, Mark C. Kuzyk, and Hailin Wang
Department of Physics and Oregon Center for Optics, University of Oregon, Eugene, Oregon 97403, USA
(Received 1 April 2013; published 28 May 2013)

We report an experimental study of transient optomechanically induced transparency (OMIT) using a silica microsphere as a model optomechanical resonator. Transient OMIT processes were probed with a time-gated heterodyne detection technique. OMIT spectral responses were also measured as the OMIT process evolved toward the steady state. The transient OMIT behaviors observed are in good agreement with theoretical calculations based on the coupled-oscillator model. Specifically, the characteristic time scale for establishing the OMIT process is determined by the optomechanical cooperativity as well as the mechanical damping rate.

DOI: 10.1103/PhysRevA.87.055802 PACS number(s): 42.50.Wk, 03.67.Hk, 07.10.Cm

I. INTRODUCTION

Optomechanically induced transparency (OMIT) is the optomechanical analog of the well-known phenomenon of electromagnetically induced transparency (EIT) [1]. OMIT has been realized in a variety of optomechanical and electromechanical resonators under continuous-wave optical excitations [2–5]. EIT is of central importance to a variety of nonlinear and quantum optical processes [6–9]. Similarly, OMIT also plays an essential role in optomechanical processes such as optomechanical light storage [10,11] and optomechanical dark modes [12–15]. For many of these processes, OMIT takes place under transient, instead of continuous-wave, optical excitations.

In an optomechanical resonator, circulating optical fields couple to a mechanical mode of the resonator via radiation pressure forces [16,17]. Cavity optomechanics has been explored in a variety of macro-, micro-, and nano-optical systems [18,19]. Experimental studies of optomechanical processes in these systems have led to the realization of a number of remarkable coherent or quantum optical phenomena. In addition to the OMIT-related processes discussed above, these phenomena also include the strong coupling between an optical and a mechanical mode [4,20,21], the coherent interconversion between optical and mechanical modes in the classical or the quantum regime [10,21,22], optomechanics-based wavelength conversion [15,23–27], and more recently the observation of radiation pressure shot noise [28].

For OMIT, a signal field at the optical resonance and a control field at one mechanical frequency, ω_m, below the optical resonance excite a coherent mechanical oscillation through optomechanical coupling. Anti-Stokes scattering of the control field off this mechanical excitation then induces an intracavity optical field at the cavity resonance. Destructive interference between the intracavity field induced by the anti-Stokes scattering and that generated directly by the incident signal prevents the excitation of the optical mode, leading to the OMIT, as demonstrated in earlier experimental studies [2–5].

In this Brief Report, we report an experimental study of transient OMIT processes using a silica microsphere as a model optomechanical resonator. By using a time-gated detection technique, we are able to directly probe the transient OMIT process, and also measure the OMIT spectral response as the system evolves toward the steady state. The transient OMIT processes observed in our experiments are in good agreement with theoretical calculations based on the coupled-oscillator model.

II. EXPERIMENTAL SETUP

For the transient OMIT experiment, optical fields in a whispering gallery mode (WGM) of a silica microsphere were coupled to the (1, 0) radial-breathing mechanical mode of the silica microsphere [29–31]. The WGM was excited through the evanescent field of a tapered optical fiber. Both the silica microsphere and the tapered fiber were held in an enclosed chamber filled with helium gas in order to avoid degradation of optical Q factors. As shown schematically in Figs. 1(a) and 1(b), the control pulse was fixed at ω_m below a given WGM resonance and the incident signal pulse was tuned to near the WGM resonance. Both the control and the signal came from a single-frequency Ti:sapphire ring laser with $\lambda \sim 800$ nm and with its frequency locked to the WGM resonance using the Pound-Drever-Hall technique. As illustrated in the schematic of the experimental setup in Fig. 1(c), the control pulse was derived from the first-order diffraction from an acousto-optic modulator (AOM). The control pulse also propagated through an electro-optic modulator (EOM). The blue sideband generated from the electro-optic phase modulator served as the signal pulse. For the experimental results reported here, both the control and the signal pulses were square shaped, with the same timing and with a duration of 8 μs.

Heterodyne detection was used for the measurement of the optical emission from the microsphere near the WGM resonance, with the control pulse serving as the local oscillator. Since the incident signal pulse is generated directly from the local oscillator with a pure phase modulation, the heterodyne detection is not sensitive to the transmitted signal pulse that is not emitted from the optical resonator. In this regard, the heterodyne detection directly measures the power of the intracavity optical field. Similar techniques were also used in earlier OMIT and optomechanical light storage studies [2,3,10]. The transient behavior of the optical emission was probed with a spectrum analyzer operating in a time-gated detection mode (see Fig. 1(b) and also Ref. [10]), with the time resolution set by the resolution bandwidth (3 MHz) as well as the detection gate length (0.5 μs).

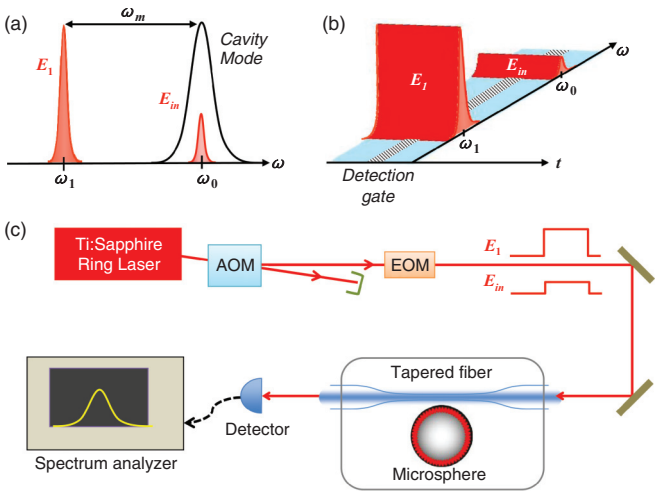

FIG. 1. (Color online) (a) and (b) Schematics of the spectral position and timing for the control and signal pulses used in the OMIT experiment. The shaded area in (b) shows the timing of the detection gate. (c) Schematic of the experimental setup. The silica microsphere and the tapered fiber were held in a chamber filled with helium gas in order to avoid contamination.

III. EXPERIMENTAL RESULTS

The experiments were carried out at room temperature using a silica microsphere with a diameter near 30 μm and with $(\omega_m, \gamma_m, \kappa)/2\pi = (160.9, 0.096, 20)$ MHz, where γ_m and κ are the mechanical and optical damping rate, respectively. Figure 2 shows the transient OMIT responses, for which the peak power (1.6 mW) of the incident control pulse corresponds to an optomechanical coupling rate, $G/2\pi = 0.45$ MHz, as determined from a separate OMIT experiment under the steady-state condition. The peak power for the incident signal pulse is 0.01 mW. Figure 2(a) plots the optical emission power from the WGM as a function of the timing, t_d, of the detection gate, with the frequency of the signal pulse tuned to the given WGM resonance. The emission power decreases with increasing t_d, approaching the steady state toward the end of the 8-μs signal pulse. Figure 2(b) shows the emission power as a function of the detuning, δ, between the signal pulse and the control pulse, obtained at various fixed timings for the detection gate. The dip in the emission power observed near $\delta = \omega_m$ indicates the underlying OMIT process. Complete OMIT spectra covering the entire spectral range of the cavity resonance under or near the steady-state condition were shown in an earlier study [15]. Figure 2(c) shows the spectral linewidth of the OMIT dip derived from Fig. 2(b) as a function of the timing of the detection gate. For comparison with theoretical calculations, optical emission powers in Fig. 2 are normalized to that obtained in the absence of the control and with the signal pulse at the WGM resonance. The emission powers in Fig. 2 obtained at $\delta = \omega_m$ thus represent the relative depth of the OMIT dip. Together, Figs. 2(a)–2(c) provide detailed information on how the OMIT process develops and evolves in the time domain.

The dependence of the transient OMIT response on the optomechanical coupling rate is presented in Fig. 3. Figure 3(a) plots the optical emission power as a function of the timing for the detection gate, obtained at various powers for the control

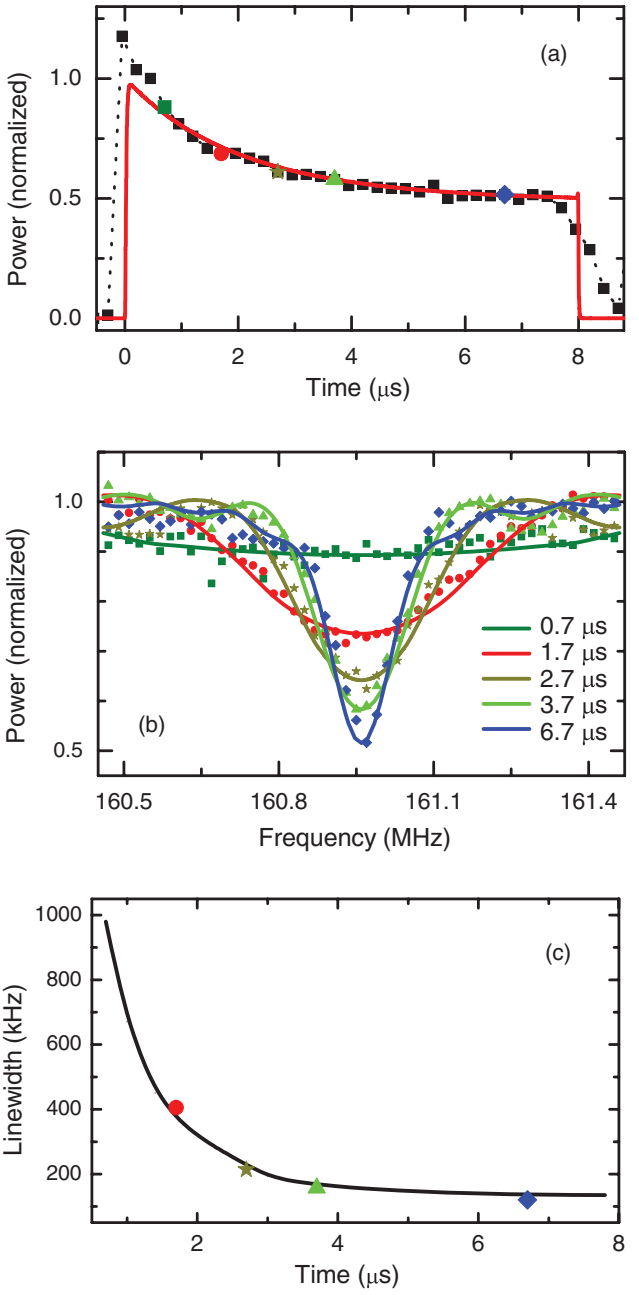

FIG. 2. (Color online) (a) Emission power from the WGM as a function of the timing of the detection gate, obtained with the signal pulse at the WGM resonance. (b) Emission power from the WGM as a function of the detuning between the signal and control, obtained at various timings for the detection gate as indicated in the figure. For both (a) and (b), the emission powers are normalized to that obtained in the absence of the control and with the signal pulse at the WGM resonance. Different symbols are also used to indicate the timing of the detection gate. (c) The spectral linewidth of the OMIT dip as a function of the timing of the detection gate derived from (b). The solid lines are results of the theoretical calculations discussed in the text.

pulse and under otherwise the same condition as Fig. 2(a). Figure 3(b) shows the emission power as a function of the detuning between the signal pulse and WGM resonance, obtained with the detection gate positioned at $t_d = 6.7$ μs. The spectral linewidth of the OMIT dip and the emission

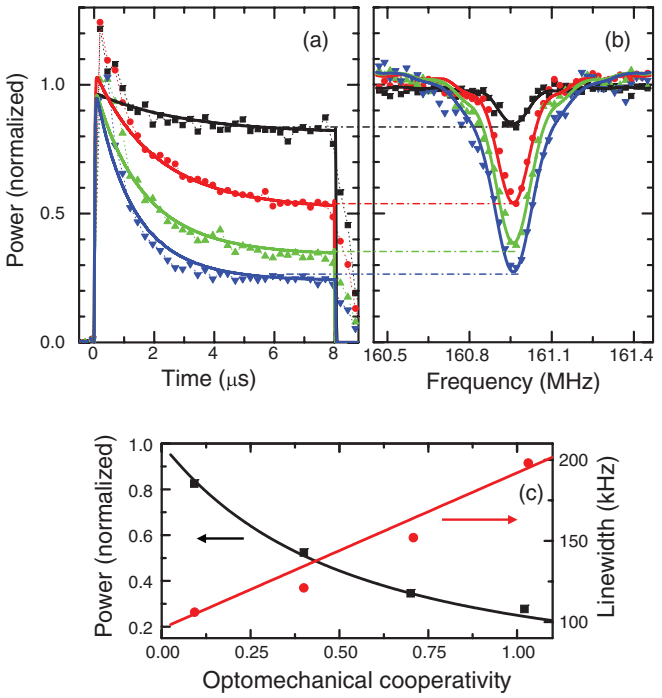

FIG. 3. (Color online) (a) Emission power from the WGM as a function of the timing of the detection gate, obtained with the signal pulse at the WGM resonance. From top to bottom, the incident control power used is 0.4, 1.6, 2.9, 4.8 mW, corresponding to $G/2\pi = 0.2, 0.45, 0.58, 0.7$ MHz, respectively. (b) Emission power from the WGM as a function of the detuning between the signal and control, obtained at $t_d = 6.7$ μs. Other conditions are the same as in (a). For both (a) and (b), the emission powers are normalized to that obtained in the absence of the control and with the signal pulse at the WGM resonance, and the expected theoretical results are shown as the solid lines. (c) The spectral linewidth of the OMIT dip and the emission power with $\delta = \omega_m$ as a function of the optomechanical cooperativity, derived from (b). The solid lines in (c) show the theoretically expected steady-state values for the linewidth and emission power.

power with $\delta = \omega_m$ derived from Fig. 3(b) are given in Fig. 3(c). The experimental results are plotted as a function of the estimated optomechanical cooperativity, $C = 4G^2/\kappa\gamma_m$, a dimensionless parameter that characterizes the strength of optomechanical coupling.

IV. ANALYSIS AND DISCUSSION

The dynamics of the above two-mode optomechanical system can be described theoretically with a set of coupled-oscillator equations, in which the control field mediates the coupling between the mechanical displacement and the intracavity optical signal field. The optomechanical coupling rate is given by $G = g_{\rm om} x_{\rm zpf}\sqrt{n_c}$ where $g_{\rm om} = d\omega/dx$ is the optomechanical coupling coefficient, $x_{\rm zpf} = \sqrt{\hbar/2m\omega_m}$ is the zero-point fluctuation for the mechanical oscillator, and n_c is the intracavity photon number for the control. In the resolved sideband limit ($\omega_m \gg \kappa$) and with the control field fixed at one mechanical frequency below the cavity resonance, the coupled-oscillator equations are given by

$$\begin{aligned}\dot{\alpha} &= \left[i(\omega_{\rm in} - \omega_0) - \frac{\kappa}{2}\right]\alpha - iG\beta + \sqrt{\kappa^{\rm ext}}\,A_{\rm in},\\ \dot{\beta} &= \left[i(\omega_{\rm in} - \omega_0) - \frac{\gamma_m}{2}\right]\beta - iG\alpha,\end{aligned} \tag{1}$$

where α and β are the complex optical signal field and mechanical displacement in the respective rotating frames, $\omega_{\rm in}$ and $A_{\rm in}$ are the frequency and amplitude of the incident optical signal field, respectively, with $A_{\rm in}$ being normalized such that $I_{\rm in} = |A_{\rm in}|^2$ is the input photon flux, and $\kappa^{\rm ext}$ is the effective output coupling rate of the signal field. Note that α and β are normalized such that $|\alpha|^2$ is the intracavity photon number and $|\beta|^2$ is the phonon number. In the steady state, the intracavity optical signal field is then given by

$$\alpha = -\frac{(i\Delta - \gamma_m/2)}{(i\Delta - \kappa/2)(i\Delta - \gamma_m/2) + G^2}\sqrt{\kappa^{\rm ext}}A_{\rm in}, \tag{2}$$

where $\Delta = \omega_{\rm in} - \omega_0 = \delta - \omega_m$. In the limit that $\gamma_m \ll \kappa$, the width of the OMIT dip is determined by $\gamma_m + 4G^2/\kappa = (1 + C)\gamma_m$. The relative depth of the OMIT dip is given by $1/(1 + C)^2$.

The experimental results shown in Figs. 2 and 3 are in good agreement with theoretical calculations using the coupled-oscillator model. Except for Fig. 3(c), the solid lines in Figs. 2 and 3 plot the theoretical calculations on the transient OMIT process based on the numerical solution to Eq. (1), with all parameters, except for G, determined independently from the experiment. The solid lines in Fig. 3(c) show the theoretical results for the steady-state OMIT response. Note that there are significant distortions in the gated detection when the gate is positioned at the leading or trailing edge of the pulse due to the nature of the gated detection of the spectrum analyzer, leading to deviations between the experiment and theory near the edges of the signal pulse [see Figs. 2(a) and 3(a)].

We now analyze in more detail the experimental results in Figs. 2 and 3. Figure 2 highlights that as the OMIT process evolves with increasing t_d, the decrease in the emission power from the WGM shown in Fig. 2(a) is correlated with a sharpening of the OMIT dip shown in Fig. 2(b). At relatively small t_d, the spectral linewidth of the OMIT dip scales inversely with t_d [see Fig. 2(c)]. In this limit, the linewidth of the OMIT dip is simply determined by the effective duration of the signal pulse that is subject to the measurement. With increasing t_d, the dynamics of the mechanical excitation becomes important. As discussed earlier, the OMIT arises from the anti-Stokes scattering of the intracavity control field off the coherent mechanical excitation induced by the control and signal. In the limit that $\gamma_m \ll \kappa$, the characteristic time scale for the mechanical excitation is $[(1 + C)\gamma_m]^{-1}$, with $4G^2/\kappa = C\gamma_m$ being the damping rate induced by the optomechanical coupling or the radiation pressure cooling rate [32,33]. This time scale is also expected to be the characteristic time scale for the establishment of the OMIT process. As the OMIT process evolves toward the steady state, the width of the OMIT dip as well as the emission power obtained with $\delta = \omega_m$ decreases monotonically to approach their steady-state values, as shown in Fig. 2(c). Note that for the experiment in

Fig. 2, the optomechanical cooperativity is estimated to be $C = 0.4$.

As shown in Fig. 3(a), with increasing control power and thus increasing optomechanical cooperativity, the emission from the WGM decreases and reaches the steady-state value in a shorter time scale. For a more detailed analysis, Fig. 3(c) also compares the spectral width and the relative depth of the OMIT dip measured at $t_d = 6.7$ μs and derived from Fig. 3(b) with the theoretically expected steady-state values. As expected from the transient OMIT response shown in Fig. 3(a), both the spectral width and the relative depth reach the steady-state value at $t_d = 6.7$ μs even when the optomechanical cooperativity is much smaller than 1. In this limit, the characteristic time scale for the mechanical excitation and the OMIT process is simply the intrinsic mechanical damping time. Overall, the experimental results shown in Figs. 2 and 3 also indicate a good agreement between the time domain and spectral domain measurements.

V. CONCLUSION

In summary, experimental studies of OMIT responses probed with a time-gated detection technique provide detailed information on the transient behavior of OMIT and especially on the evolution of the OMIT process toward the steady state. These studies confirm that the characteristic time scale for establishing OMIT is $[(1 + C)\gamma_m]^{-1}$. This time scale should also be the characteristic time scale for the use of OMIT in transient optomechanical processes, such as the coherent conversion between optical and mechanical modes or between two optical modes via an optomechanical dark mode.

ACKNOWLEDGMENTS

This work is supported by NSF and by the DARPA-MTO ORCHID program through a grant from AFOSR.

[1] G. S. Agarwal and S. M. Huang, Phys. Rev. A **81**, 041803 (2010).
[2] S. Weis, R. Riviere, S. Deleglise, E. Gavartin, O. Arcizet, A. Schliesser, and T. J. Kippenberg, Science **330**, 1520 (2010).
[3] A. H. Safavi-Naeini, T. P. M. Alegre, J. Chan, M. Eichenfield, M. Winger, Q. Lin, J. T. Hill, D. E. Chang, and O. Painter, Nature **472**, 69 (2011).
[4] J. D. Teufel, D. Li, M. S. Allman, K. Cicak, A. J. Sirois, J. D. Whittaker, and R. W. Simmonds, Nature **471**, 204 (2011).
[5] M. Karuza, C. Biancofiore, C. Molinelli, M. Galassi, R. Natali, P. Tombesi, G. Di Giuseppe, and D. Vitali, arXiv:1209.1352.
[6] E. Arimondo, Prog. Opt. **35**, 257 (1996).
[7] S. E. Harris, Phys. Today **50**, 36 (1997).
[8] M. D. Lukin, Rev. Mod. Phys. **75**, 457 (2003).
[9] M. O. Scully and M. S. Zubairy, *Quantum Optics* (Cambridge University Press, Cambridge, 1997).
[10] V. Fiore, Y. Yang, M. C. Kuzyk, R. Barbour, L. Tian, and H. Wang, Phys. Rev. Lett. **107**, 133601 (2011).
[11] V. Fiore, C. H. Dong, M. C. Kuzyk, and H. L. Wang, Phys. Rev. A **87**, 023812 (2013).
[12] Y. D. Wang and A. A. Clerk, Phys. Rev. Lett. **108**, 153603 (2012).
[13] Y. D. Wang and A. A. Clerk, New J. Phys. **14**, 105010 (2012).
[14] L. Tian, Phys. Rev. Lett. **108**, 153604 (2012).
[15] C. Dong, V. Fiore, M. C. Kuzyk, and H. Wang, Science **338**, 1609 (2012).
[16] V. B. Braginsky, *Measurement of Weak Forces in Physics Experiments* (University of Chicago Press, Chicago, 1977).
[17] A. Dorsel, J. D. Mccullen, P. Meystre, E. Vignes, and H. Walther, Phys. Rev. Lett. **51**, 1550 (1983).
[18] T. J. Kippenberg and K. J. Vahala, Science **321**, 1172 (2008).
[19] M. Aspelmeyer, P. Meystre, and K. Schwab, Phys. Today **65**(7), 29 (2012).
[20] S. Groblacher, K. Hammerer, M. R. Vanner, and M. Aspelmeyer, Nature **460**, 724 (2009).
[21] E. Verhagen, S. Deleglise, S. Weis, A. Schliesser, and T. J. Kippenberg, Nature **482**, 63 (2012).
[22] T. A. Palomaki, J. W. Harlow, J. D. Teufel, R. W. Simmonds, and K. W. Lehnert, Nature **495**, 210 (2013).
[23] J. T. Hill, A. H. Safavi-Naeini, J. Chan, and O. Painter, Nat. Commun. **3**, 1196 (2012).
[24] L. Tian and H. L. Wang, Phys. Rev. A **82**, 053806 (2010).
[25] A. H. Safavi-Naeini and O. Painter, New J. Phys. **13**, 013017 (2011).
[26] C. A. Regal and K. W. Lehnert, J. Phys.: Conf. Ser. **264**, 012025 (2011).
[27] S. Barzanjeh, M. Abdi, G. J. Milburn, P. Tombesi, and D. Vitali, Phys. Rev. Lett. **109**, 130503 (2012).
[28] T. P. Purdy, R. W. Peterson, and C. A. Regal, Science **339**, 801 (2013).
[29] R. Ma, A. Schliesser, P. Del'Haye, A. Dabirian, G. Anetsberger, and T. J. Kippenberg, Opt. Lett. **32**, 2200 (2007).
[30] Y. S. Park and H. L. Wang, Nat. Phys. **5**, 489 (2009).
[31] T. Carmon, H. Rokhsari, L. Yang, T. J. Kippenberg, and K. J. Vahala, Phys. Rev. Lett. **94**, 223902 (2005).
[32] F. Marquardt, J. P. Chen, A. A. Clerk, and S. M. Girvin, Phys. Rev. Lett. **99**, 093902 (2007).
[33] I. Wilson-Rae, N. Nooshi, W. Zwerger, and T. J. Kippenberg, Phys. Rev. Lett. **99**, 093901 (2007).